16TH EUROPEAN CONFERENCE ON EARTHQUAKE ENGINEERING THESSALONIKI 18 - 21 JUNE 2018

COMPARISON OF STATIC AND DYNAMIC NON-LINEAR KINEMATIC ANALYSIS

Sander MEIJERS[1], Maria ROSALES[2]

ABSTRACT

The subject of rocking of rigid bodies due to seismic excitation has been studied since the 1980's and practical applications to out-of-plane failure of masonry walls have entered well into several national building design codes. However, consensus about the effective natural period of the kinematic system and safe limitations of its displacement capacity is lacking in those practical applications. In the present study a rigorous mathematical model of the kinematic system of two rigid blocks on top of each other in rocking motion has been set up, which builds on simpler versions in literature. The ensuing single degree-of-freedom system and geometrically non-linear problem has been solved numerically in the time domain for a number of earthquake records. It appears that the displacement capacities and allowable peak ground accelerations surpass coded values. An assessment of the reliability of walls in rocking motion as determined by the codes is made by statistical analysis of the obtained numerical results.

Keywords: Rocking; Wall; Dynamic; SDOF; Kinematic

1. INTRODUCTION

With the increase of seismic activity due to gas extraction from the subsoil in the North of The Netherlands over the past ten years, one of the subjects that has gained attention among the Dutch engineering community is the seismic capacity of unreinforced masonry walls. In particular, the out-of-plane behavior has become of great interest, as it can lead to local failure modes which can be governing in the seismic analysis, and ultimately lead to collapse of a large portion of a building.

The high out-of-plane vulnerability of typical slender unreinforced masonry walls in The Netherlands in conjunction with uncertainties regarding the actual masonry material properties, has led to the application of Non-Linear Kinematic Analysis (NLKA) in order to verify the out-of-plane capacity of an existing wall. NLKA is based on the analysis of a rocking mechanism which represents the failure mode that is observed when a vertical-spanning unreinforced masonry wall fails out-of-plane due to formation of cracks at bottom, top and mid-height of the wall. As such it is independent of the material properties. The analysis of the stability of the system leads to a design deformation capacity, defined as a fraction of the maximum deformation of the system before becoming unstable. In this way, the deformation capacity can be checked against a target displacement demand derived from the response spectrum.

However, it is believed that the actual displacement capacity of the walls can actually be larger than this calculated value. One possible reason for this is that the calculation for this displacement capacity is done in a static way, while in practice the earthquake loading will be applied dynamically. Therefore, both the maximum deformation of the system, and the factor used to determine the ultimate capacity from the instability displacement (which can also vary depending on the chosen seismic code), might be on the conservative side.

[1]Dr.ir., AT&R Dept., Royal HaskoningDHV, Rotterdam, The Netherlands, sander.meijers@rhdhv.com
[2]ir., AT&R Dept., Royal HaskoningDHV, The Netherlands, maria.rosales.gonzalez@rhdhv.com

In order to further investigate this matter, a differential equation that models the dynamic rocking behavior of a vertical spanning masonry wall has been derived and numerically solved. Numerical results have been obtained for a large number of earthquake time-histories matching a single response spectrum set and a large number of peak ground accelerations (PGAs). The present paper shows the results of this comparison between static and dynamic NLKA in a statistical way.

2. MODEL FOR DYNAMIC NON-LINEAR KINEMATIC ANALYSIS

The model consists of two blocks (1 and 2) of width b and heights h_1 and h_2, placed one on top of the other. The blocks can rotate such that the bottommost corner (A) of block 1 can be assumed to remain hinged to the ground, while the bottommost corner (C) of block 2 is hinged to the topmost corner of block 1. The topmost corner (B) of block 1 is assumed to be restrained in the horizontal direction.

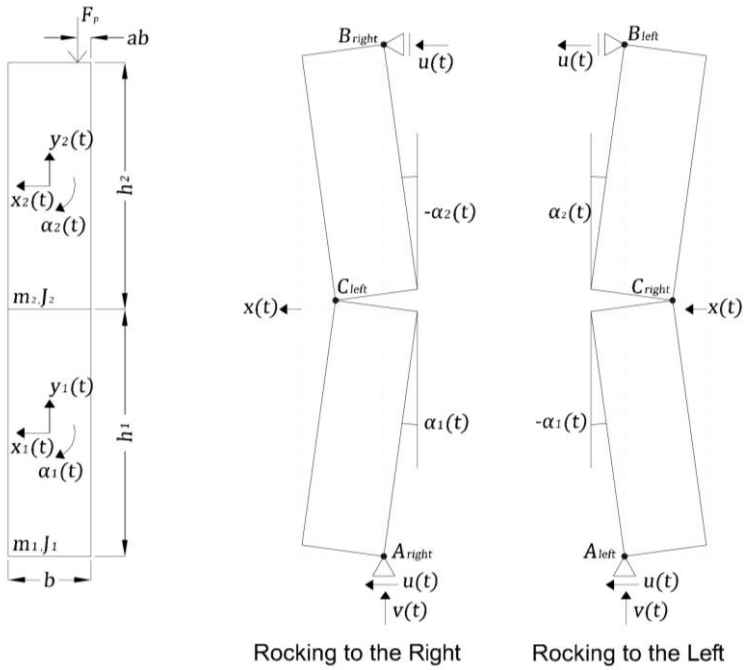

Figure 1. Depiction of model and degrees of freedom for rocking to the right and to the left

It is assumed that a horizontal and vertical ground displacement (u and v respectively) is prescribed on the supports at A and B. Additionally, an overburden load is applied at a distance ab from the top right corner of block 2.

A depiction of the model is shown in Figure 1. The corresponding equilibrium equations and kinematic relations are listed in Table 1, accounting for both cases when the system is rocking to the left and to the right. In summary there are:

- 6 equilibrium equations
- 5 unknown forces: R_{Ax}, R_{Ay}, R_{Bx}, F_{Cx} and F_{Cy} at points A, B and C
- 6 unknown displacements and rotations: x_1, y_1, x_2, y_2, α_1 and α_2; they are interdependent and can be replaced by a single generalized degree-of-freedom (DOF) x

Table 1. Equilibrium equations, kinematic relations, and definition of generalized displacement pertaining to the model for dynamic kinematic analysis. For the rigid blocks the rotational inertia J_i equals $m_i(b^2 + h_i^2)/12$.

Type	DOF	Rocking to the left	Rocking to the right
Equilibrium	$m_1\ddot{x}_1$	$-R_{Ax} + F_{Cx}$	Idem
	$m_1\ddot{y}_1$	$-m_1 g + F_{Cy}$	Idem
	$J_1\ddot{\alpha}_1$	$+F_{Cx}\left(\frac{b}{2}\sin\alpha_1 - \frac{h_1}{2}\cos\alpha_1\right)$ $-F_{Cy}\left(\frac{b}{2}\cos\alpha_1 + \frac{h_1}{2}\sin\alpha_1\right)$ $+R_{Ax}\left(\frac{b}{2}\sin\alpha_1 - \frac{h_1}{2}\cos\alpha_1\right)$ $-R_{Ay}\left(\frac{b}{2}\cos\alpha_1 + \frac{h_1}{2}\sin\alpha_1\right)$	$-F_{Cx}\left(\frac{b}{2}\sin\alpha_1 + \frac{h_1}{2}\cos\alpha_1\right)$ $+F_{Cy}\left(\frac{b}{2}\cos\alpha_1 - \frac{h_1}{2}\sin\alpha_1\right)$ $-R_{Ax}\left(\frac{b}{2}\sin\alpha_1 + \frac{h_1}{2}\cos\alpha_1\right)$ $+R_{Ay}\left(\frac{b}{2}\cos\alpha_1 - \frac{h_1}{2}\sin\alpha_1\right)$
	$m_2\ddot{x}_2$	$+R_{Bx} - F_{Cx}$	Idem
	$m_2\ddot{y}_2$	$-F_p - m_2 g - F_{Cy}$	Idem
	$J_2\ddot{\alpha}_2$	$-R_{Bx}\left(\frac{b}{2}\sin\alpha_2 + \frac{h_2}{2}\cos\alpha_2\right)$ $+F_p\left(\frac{b}{2}(1-2a)\cos\alpha_2 + \frac{h_2}{2}\sin\alpha_2\right)$ $-F_{Cx}\left(\frac{b}{2}\sin\alpha_2 + \frac{h_2}{2}\cos\alpha_2\right)$ $+F_{Cy}\left(\frac{b}{2}\cos\alpha_2 - \frac{h_2}{2}\sin\alpha_2\right)$	$R_{Bx}\left(\frac{b}{2}\sin\alpha_2 - \frac{h_2}{2}\cos\alpha_2\right)$ $+F_p\left(\frac{b}{2}(1-2a)\cos\alpha_2 + \frac{h_2}{2}\sin\alpha_2\right)$ $+F_{Cx}\left(\frac{b}{2}\sin\alpha_2 - \frac{h_2}{2}\cos\alpha_2\right)$ $-F_{Cy}\left(\frac{b}{2}\cos\alpha_2 + \frac{h_2}{2}\sin\alpha_2\right)$
Kinematic relations	x_1	$u - \frac{b}{2}\cos\alpha_1 - \frac{h_1}{2}\sin\alpha_1$	$u + \frac{b}{2}\cos\alpha_1 - \frac{h_1}{2}\sin\alpha_1$
	y_1	$v - \frac{b}{2}\sin\alpha_1 + \frac{h_1}{2}\cos\alpha_1$	$v + \frac{b}{2}\sin\alpha_1 + \frac{h_1}{2}\cos\alpha_1$
	x_2	$u - \frac{b}{2}\cos\alpha_2 + \frac{h_2}{2}\sin\alpha_2$	$u + \frac{b}{2}\cos\alpha_2 + \frac{h_2}{2}\sin\alpha_2$
	y_2	$v + \frac{b}{2}\sin\alpha_2 + \frac{h_2}{2}\cos\alpha_2$	$v - \frac{b}{2}\sin\alpha_2 + \frac{h_2}{2}\cos\alpha_2$
	Implicit	$-b\sin\alpha_1 + h_1\cos\alpha_1$ $-b\cos\alpha_1 - h_1\sin\alpha_1 =$ $-b\cos\alpha_2 + h_2\sin\alpha_2$	$+b\sin\alpha_1 + h_1\cos\alpha_1$ $b\cos\alpha_1 - h_1\sin\alpha_1 =$ $b\cos\alpha_2 + h_2\sin\alpha_2$
Generalized relative displacement	x	$-b\cos\alpha_1 - h_1\sin\alpha_1 + b =$ $-b\cos\alpha_2 + h_2\sin\alpha_2 + b$ (positive)	$b\cos\alpha_1 - h_1\sin\alpha_1 - b =$ $b\cos\alpha_2 + h_2\sin\alpha_2 - b$ (negative)
Small angle approximation $\cos\alpha_i = 1$ $\sin\alpha_i = \alpha_i$	x	$-h_1\alpha_1 = h_2\alpha_2$	Idem
	$\ddot{x}_1$	$\ddot{u} - \frac{h_1}{2}\ddot{\alpha}_1 = \ddot{u} + \frac{\ddot{x}}{2}$	Idem
	$\ddot{y}_1$	$\ddot{v} - \frac{b}{2}\ddot{\alpha}_1 = \ddot{v} + \frac{b\ddot{x}}{2h_1}$	$\ddot{v} + \frac{b}{2}\ddot{\alpha}_1 = \ddot{v} - \frac{b\ddot{x}}{2h_1}$
	$\ddot{x}_2$	$\ddot{u} + \frac{h_2}{2}\ddot{\alpha}_2 = \ddot{u} + \frac{\ddot{x}}{2}$	Idem
	$\ddot{y}_2$	$\ddot{v} - b\ddot{\alpha}_1 + \frac{b}{2}\ddot{\alpha}_2 =$ $\ddot{v} + \left(\frac{b}{h_1} + \frac{b}{2h_2}\right)\ddot{x}$	$\ddot{v} + b\ddot{\alpha}_1 - \frac{b}{2}\ddot{\alpha}_2 =$ $\ddot{v} - \left(\frac{b}{h_1} + \frac{b}{2h_2}\right)\ddot{x}$

In general only one differential equation remains for this single degree-of-freedom (SDOF) system, which for the small angle approximation has the following form:

$$(p_1 + p_2 x + p_3 x^2)\frac{d^2x}{dt^2} + (p_4 + p_5 x)x = p_6 \tag{1}$$

where the coefficients p_i are defined as:

$$p_1 = \frac{J_1}{h_1^2} + \frac{J_2}{h_2^2} + \frac{m_1}{4} + \frac{m_2}{4} + \frac{b^2 m_1}{4h_1^2} + \frac{b^2 m_2}{4h_2^2} + \frac{b^2 m_2}{h_1 h_2} + \frac{b^2 m_2}{h_1^2} \tag{2}$$

$$p_2 = sgn(x)\left(b\frac{J_1+J_2}{h_1^2 h_2^2} - \frac{3bm_2}{4h_1^2} + \frac{bm_1}{4h_2^2} - \frac{bm_2}{h_1 h_2} + b^3\left(\frac{m_1}{4h_1^2 h_2^2} + \frac{m_2}{2h_1 h_2^3} + \frac{5m_2}{4h_1^2 h_2^2} + \frac{m_2}{2h_1^3 h_2}\right)\right) \tag{3}$$

$$p_3 = -b^2 m_2\left(\frac{1}{2h_1 h_2^3} + \frac{1}{h_1^2 h_2^2} + \frac{1}{2h_1^3 h_2}\right) \tag{4}$$

$$p_4 = -F_p\left(\frac{1}{h_1} + \frac{1}{h_2} - \frac{b^2}{h_1 h_2}\left(\frac{d}{h_1} + \frac{1}{h_2}\right)\right) - (g + \ddot{v})\left(\frac{m_2}{2h_2} + \frac{m_2}{h_1} + \frac{m_1}{2h_1} - \frac{b^2}{h_1 h_2}\left(\frac{m_2}{2h_1} + \frac{m_2}{h_2} + \frac{m_1}{2h_2}\right)\right) + sgn(x)\frac{\ddot{u}}{2}b(m_1 + m_2)\left(\frac{1}{h_1^2} + \frac{1}{h_2^2}\right) \tag{5}$$

$$p_5 = \left(b^2\frac{m_1+m_2}{2h_1^2 h_2^2}\ddot{u} - sgn(x)\left(bF_p\left(\frac{1}{h_1 h_2^2} + \frac{1}{h_1^2 h_2}\right) + (g + \ddot{v})b\left(\frac{m_1}{2h_1 h_2^2} + \frac{m_2}{h_1 h_2^2} + \frac{m_2}{2h_1^2 h_2}\right)\right)\right) \tag{6}$$

$$p_6 = -sgn(x)F_p b\left(\frac{1}{h_1} + \frac{d}{h_2}\right) - \frac{\ddot{u}}{2}(m_1 + m_2) - sgn(x)b(g + \ddot{v})\left(\frac{m_1}{2h_1} + \frac{m_2}{2h_2} + \frac{m_2}{h_1}\right) \tag{7}$$

where $d = 1 - a$ for $x < 0$ and $d = 1 - a'$ for $x > 0$, and $sgn(x)$ is the sign function. The behavior of the overburden load is determined by $a' = 1 - a$ if the position of the overburden load remains still, and $a' = a$ if the overburden load switches its position (i.e. mirrored) due to the rocking of the system. The stiffness terms p_4 and $p_5 x$ are generally negative, which characterizes the instablity of the SDOF system.

A routine has been programmed using Newmark implicit time marching (with β = 0.25 and γ = 0.50) and Newton-Raphson equilibrium iteration to numerically solve the seismic response of this SDOF system in the time domain.

2.1 Rocking motion and energy dissipation

The transition between rocking to the left and rocking to the right (i.e. when the supports change between points C_{right} and C_{left}) occurs when α_1 = 0 and α_2 = 0, so when x = 0, namely the zero-crossing. The change of supports during the rocking motion is only possible if the collision that occurs during the impact is inelastic, therefore, the kinetic energy is not conserved. A coefficient of restitution r is defined as the ratio of kinetic energies immediately before and after the impact, which reduces to the ratio of rotational kinetic energies, as the translational energy at this moment is zero (relative to the defined reference system):

$$r = \frac{\frac{1}{2}J_1\dot{\alpha}_{1,after}{}^2 + \frac{1}{2}J_2\dot{\alpha}_{2,after}{}^2}{\frac{1}{2}J_1\dot{\alpha}_{1,before}{}^2 + \frac{1}{2}J_2\dot{\alpha}_{2,before}{}^2} \tag{8}$$

Clearly, it holds that $0 \leq r \leq 1$. Using the definition of the generalized relative displacement according to Table 1, it follows that:

$$r = \frac{\frac{1}{2}\left(\frac{J_1}{h_1^2}+\frac{J_2}{h_2^2}\right)\dot{x}_{after}{}^2}{\frac{1}{2}\left(\frac{J_1}{h_1^2}+\frac{J_2}{h_2^2}\right)\dot{x}_{before}{}^2} = \frac{\dot{x}_{after}{}^2}{\dot{x}_{before}{}^2} \tag{9}$$

Therefore, the velocity $\dot{x}$ immediately after the impact can be written as:

$$\dot{x}_{after} = \sqrt{r}\,\dot{x}_{before} \tag{10}$$

Equation 10 applies for impacts in both directions (left to right and right to left). Since the generalized acceleration $\ddot{x}$ is the fundamental unknown in Newmark implicit time marching, it is necessary to also redefine this acceleration just after the impact as a function of the coefficient of restitution. Therefore, it is considered that at the instant of the zero-crossing it holds that:

$$M\ddot{x}_{t+\Delta t} + C\dot{x}_{t+\Delta t} = F_{t+\Delta t} \tag{11}$$

with C as the damping coefficient, $M = p_1 + p_2 x + p_3 x^2$ and $F_{t+\Delta t} = -p_6$. Time t is just before the zero-crossing and time $t + \Delta t$ just after it. In general the zero-crossing occurs in between two consecutive time steps used in the numerical solution process, as illustrated in Figure 2.

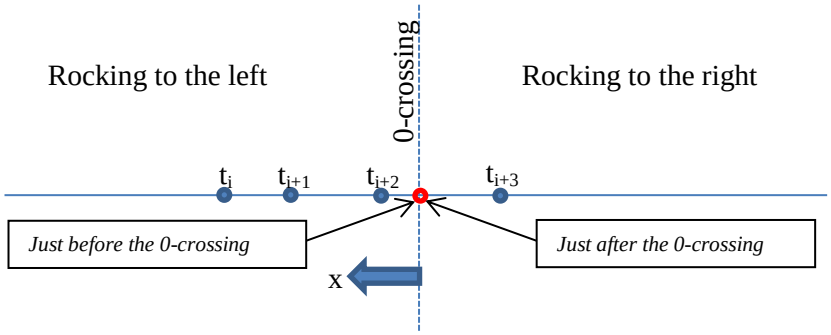

Figure 2. Determination of the time of impact. Regular time steps are denoted by t_i, t_{i+1}, t_{i+2} and t_{i+3}.

The zero-crossing is a unique state between rocking to the left and rocking to the right. Using Newmark implicit time marching it holds that:

$$\dot{x}_{t+\Delta t} = \dot{x}_t + \Delta t\left((1-\gamma)\ddot{x}_t + \gamma\ddot{x}_{t+\Delta t}\right) \tag{12}$$

with γ = 0.5 as Newmark's parameter. From Equation 9 it follows that the amount of energy lost at the zero-crossing equals:

$$\frac{1}{2}\left(\frac{J_1}{h_1^2}+\frac{J_2}{h_2^2}\right)\dot{x}_t^2(1-r) = \int_t^{t+\Delta t} C\dot{x}^2 dt \approx C\dot{x}_t^2\Delta t \tag{13}$$

Elimination of the time increment Δt in the last two equations yields the following definition of the damping coefficient:

$$C = \frac{\frac{1}{2}\left(\frac{J_1}{h_1^2}+\frac{J_2}{h_2^2}\right)(1-r)\left((1-\gamma)\ddot{x}_t+\gamma\ddot{x}_{t+\Delta t}\right)}{\dot{x}_t\left(\sqrt{r}-1\right)} \tag{14}$$

As the damping coefficient must be positive and $r < 1$, the counter must be positive for negative velocities $\dot{x}_t$ and vice versa. The acceleration just after the zero-crossing can then be derived by substitution of the expression for the damping coefficient into the equilibrium equation at the zero crossing (using the coefficients for rocking to the new side):

$$\ddot{x}_{t+\Delta t} = \frac{F_{t+\Delta t} + M_r(1-\gamma)\ddot{x}_t}{M - M_r\gamma} \tag{15}$$

with:

$$M_r = \frac{1}{2}\left(\frac{J_1}{h_1^2} + \frac{J_2}{h_2^2}\right)\left(r + \sqrt{r}\right) \tag{16}$$

The concept of energy dissipation during rocking motion of blocks has been studied by several authors (Chatzis 2017, Makris and Roussos 1998, Yim et al. 1980, Housner 1963). If the blocks are infinitely rigid, the coefficient of restitution r is only dependent on the geometry of the blocks, and can be derived using conservation of angular momentum. However, in practice the dissipation of energy is also related to factors such as the material properties of the blocks, the quality of the mortar joints or the overburden load applied. Some authors have tried to derive this coefficient experimentally, finding that, in practice, the experimental values of r are lower than the ones obtained with a simply geometric expression, usually by factors ranging from 0.78 to 0.91 (Graziotti et al. 2016, Sorrentino 2003).

In the present paper the formula presented by Sorrentino et al. 2008 (rewritten using the current definitions of the wall properties) is used to derive the analytical value of r:

$$r_{ana} = \frac{h_1 h_2 + 2h_1^2 - 3b^2}{h_1 h_2 + 2h_1^2 + 3b^2} \tag{17}$$

The previous value is further reduced by a factor chosen as 0.9, based on the findings by previous authors:

$$r_{exp} = 0.9\, r_{ana} \tag{18}$$

Both coefficients of restitution r_{ana} and r_{exp} will be used in order to get lower and (ideal) upper bound estimates of the wall capacity.

2.2 Threshold acceleration

From Equation 1 and 7 it can be inferred that for rocking to the left ($x > 0$) to start, the force p_6 must be positive. Consequently, the horizontal ground acceleration $\ddot{u}$ must be negative and surpass the following threshold value:

$$\ddot{u} < -2\,\frac{F_p b\left(\frac{1}{h_1} + \frac{d}{h_2}\right) + b(g+\ddot{v})\left(\frac{m_1}{2h_1} + \frac{m_2}{2h_2} + \frac{m_2}{h_1}\right)}{m_1 + m_2} = -\ddot{u}_{threshold} \tag{19}$$

Analogously, for rocking to the right ($x < 0$) to start, the horizontal ground acceleration $\ddot{u}$ must be positive and it is required that $\ddot{u} > \ddot{u}_{threshold}$. So for ground accelerations between $-\ddot{u}_{threshold}$ and $+\ddot{u}_{threshold}$ the SDOF system does not move.

3. COMPARISON WITH STATIC CASE

The results from dynamic non-linear kinematic analysis with the model as described in the previous chapter can be compared to results from conventional static non-linear kinematic analysis (NLKA). In a static NLKA (NTC 2008, NZSEE 2016), the simply supported wall is modelled as an equivalent SDOF system, where the seismic displacement demand of the wall system as in Figure 1 is determined using an "effective natural period" *T*:

$$T = \sqrt{\frac{(2\pi\lambda)^2\left(\frac{b}{2}-\frac{\Psi h}{8\left(1+\frac{F_p}{W}\right)}\right)}{\left(\left(1+\frac{F_p}{W}\right)\frac{4b}{h}-\Psi\right)g(1-\lambda^2)}} \tag{20}$$

The maximum allowable out-of-plane displacement of the equivalent single degree of freedom (SDOF) system is defined as:

$$x_{eq,max} = \lambda\left(\frac{b}{2}-\frac{\Psi h}{8\left(1+\frac{F_p}{W}\right)}\right) \tag{21}$$

Where W is the total weight of the wall, h its total height and Ψ the initial inclination of the wall. The instability factor λ equals 0.6 according to NSZEE C8 (2016) and 0.4 according to NTC (2008).

From T, $x_{eq,max}$ and the applicable response spectrum, it is possible to determine the maximum allowable PGA that can be applied to the system. Figure 3 shows the resulting allowable PGA as a function of the instability factor for several slenderness ratios based on the bedrock spectrum of NPR 9998 (2015) and a thickness of 0.1 m. According to static NLKA the allowable PGA for a straight (Ψ = 0 rad) wall with a height of 3.5 m, thickness 0.1 m and no overburden load (F_p = 0 N) is 0.14g according to NTC (2008) with an effective natural period of 0.573 s, or 0.18g according to NZSEE (2016) with an effective natural period of 0.996 s.

It is a matter of interest to know what the allowable PGA would be according to dynamic NLKA for this case. For this purpose the seismic bedrock excitation time histories as defined in NPR 9998 (2015) have been applied to the dynamic NLKA model as described in the previous chapter with the parameters as listed in Table 2. These consist of eleven sets of time-histories, each for three orthogonal directions XYZ, produced by spectral matching using the response spectra of NPR 9998 (2015) as target spectra.. For the present 2-dimensional case the X and Y (horizontal) directions have been individually combined with the Z (vertical) direction. Also the response to only horizontal seismic excitation has been investigated. The bedrock response spectra of NPR 9998 (2015), along with the matched time history response spectra, are shown in Figure 4 and Figure 5.

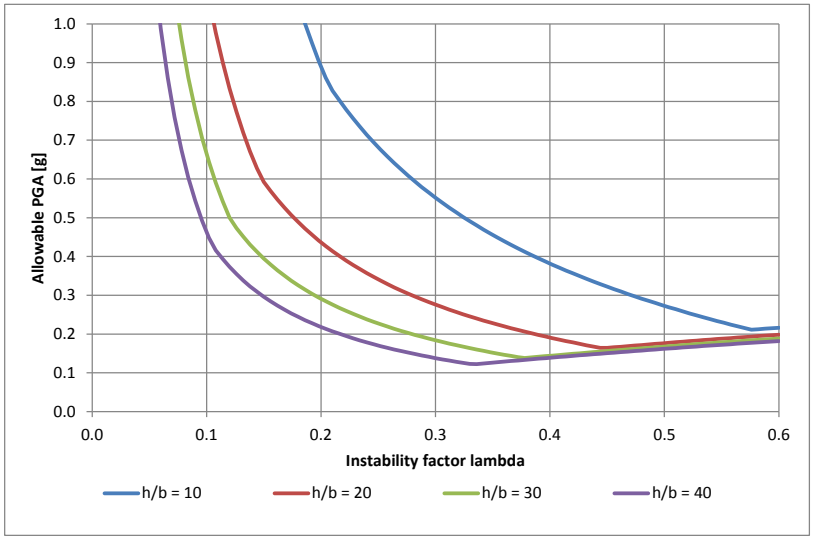

Figure 3. Allowable PGA for a straight wall without overburden according to static non-linear kinematic analysis based on the bedrock spectrum of NPR 9998 (2015) and a wall thickness of 0.1 m

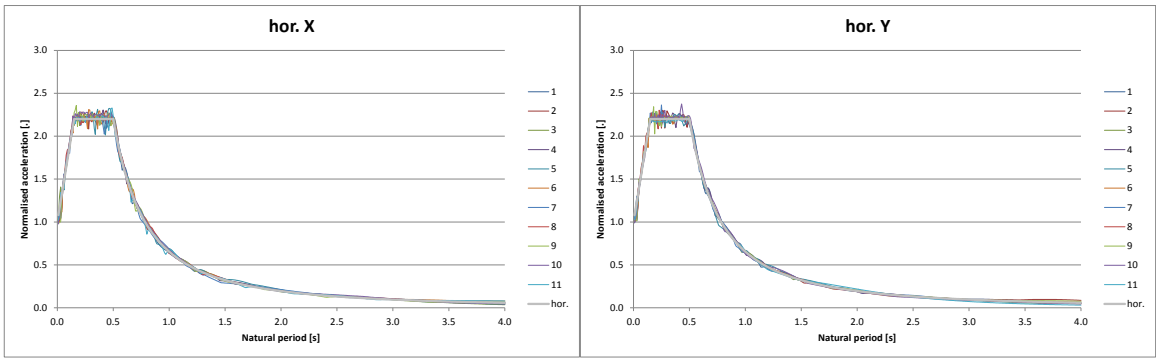

Figure 4. Response spectra and matched time-histories corresponding to the 11 horizontal X and Y time-histories as specified by NPR 9998 (2015)

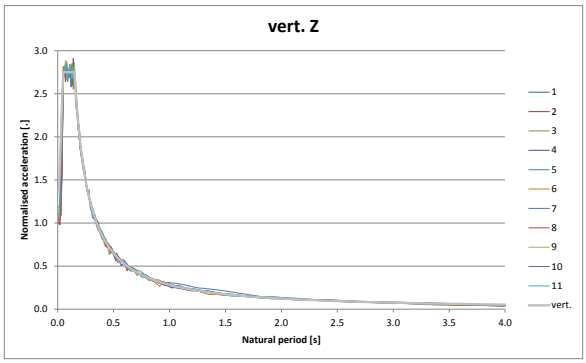

Figure 5. Response spectrum and matched time-histories corresponding to the 11 vertical Z time-histories as specified by NPR 9998 (2015)

Table 2. Properties used for the dynamic non-linear kinematic analyses.

b	ρ	h_1	h_2	a	a'	F_p	r_{ana}	r_{exp}	β	γ
m	kg/m^3	m	m	.	.	N	.		.	.
0.10	1800	1.75	1.75	0	0	0	0.993	0.894	0.25	0.50

The results of the dynamic NLKA are shown in Figure 6, Figure 7 and Figure 8. Considering a threshold acceleration of 0.11*g (without any vertical earthquake acceleration applied) for this case, the analyses have been performed for PGA's ranging from 0.11g to 0.30g with 0.01g increments. Each horizontal time-history or combination of horizontal and vertical time-histories has been scaled according to this range of PGA's. This leads to 440 analyses for horizontal seismic excitation only and another 440 analyses for the combined horizontal and vertical seismic excitation, for each of the chosen coefficient of restitution values. It was found that the non-linear terms p_2, p_3 and p_5 do not significantly affect the results for small rotation angles and can be neglected.

Rather than analyzing the individual results of each one of the analyses, the objective of this research is more related to statistically analyzing the global results, particularly in terms of whether the applied motions can cause or not a collapse of the system. For this purpose, the results for the case with both horizontal and vertical applied motions, and coefficient of restitution r_{exp}, are shown in Figure 6. It is interesting to observe also that time history combinations that cause collapse for a certain PGA scaling, may not cause collapse for a higher PGA scaling in certain cases.

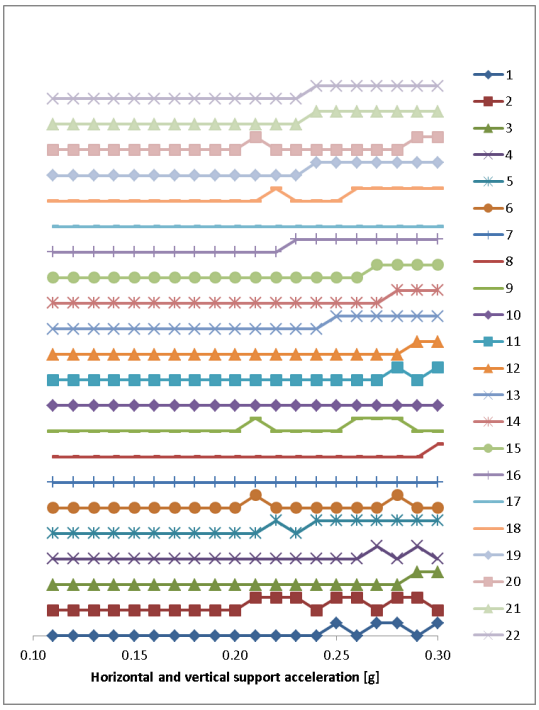

Figure 6. Collapses for the various pairs of seismic time-histories, for a straight wall with slenderness 35, thickness 0.1 m, no overburden, coefficient of restitution r_{ana} and subjected to vertical and horizontal time-histories matching the bedrock spectrum of NPR 9998 (2015). The bumps in the graphs indicate collapse.

On a first instance, the minimum PGA that led to a collapse of the system was observed for each one of the modelled cases. Additionally, for each of the used PGAs, a survival rate was found, which is defined as the number of applied time history combinations that do not lead to a collapse of the system, with respect to the total number of applied time history combinations for that particular PGA. This survival rate can be approximated by means of a cumulative normal distribution function, for which the mean and standard deviation were found by using the least squares approach. These results are summarized in Table 3. The resulting maximum displacements, compared to the survival rate and its fitted cumulative normal distribution, are shown in Figure 7 and Figure 8, for the used coefficients of restitution r_{ana} and r_{exp}, respectively.

Table 3.Obtained results for each case

Horizontal Earthquake	Vertical Earthquake	r	Minimum PGA for collapse	Fitted cumulative normal distribution PGA	
				Mean	Standard Deviation
Yes	No	r_{ana}	0.15g	0.221g	0.055g
Yes	Yes	r_{ana}	0.16g	0.219g	0.053g
Yes	No	r_{exp}	0.21g	0.268g	0.047g
Yes	Yes	r_{exp}	0.21g	0.271g	0.045g

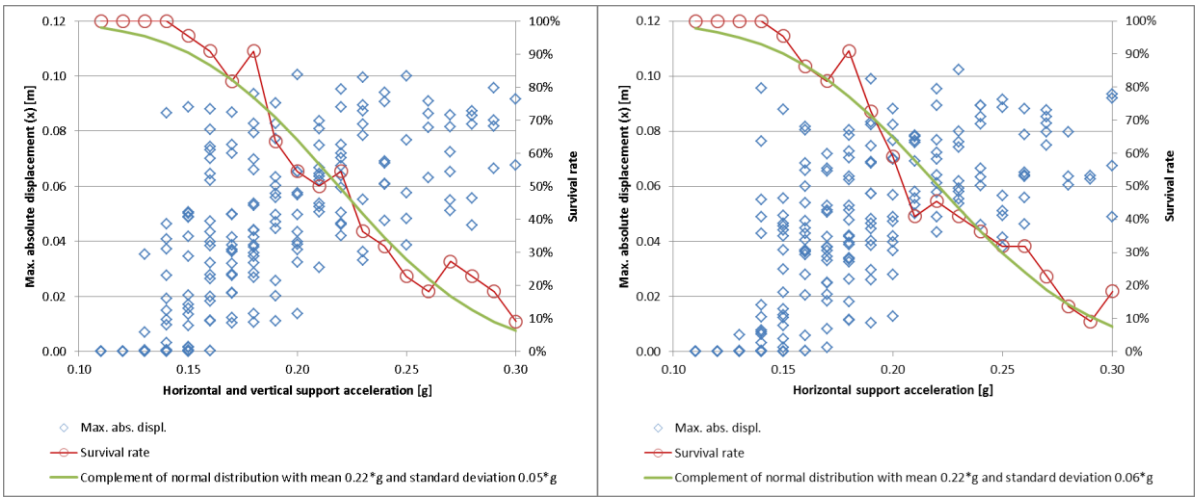

Figure 7. Results from dynamic non-linear kinematic analysis for a straight wall with slenderness 35, thickness 0.1 m, no overburden, coefficient of restitution r_{ana} and subjected to time-histories matching the bedrock spectrum of NPR 9998 (2015). Combinations with simultaneous horizontal and vertical seismic excitation are shown on the left, combinations with only horizontal seismic excitation on the right.

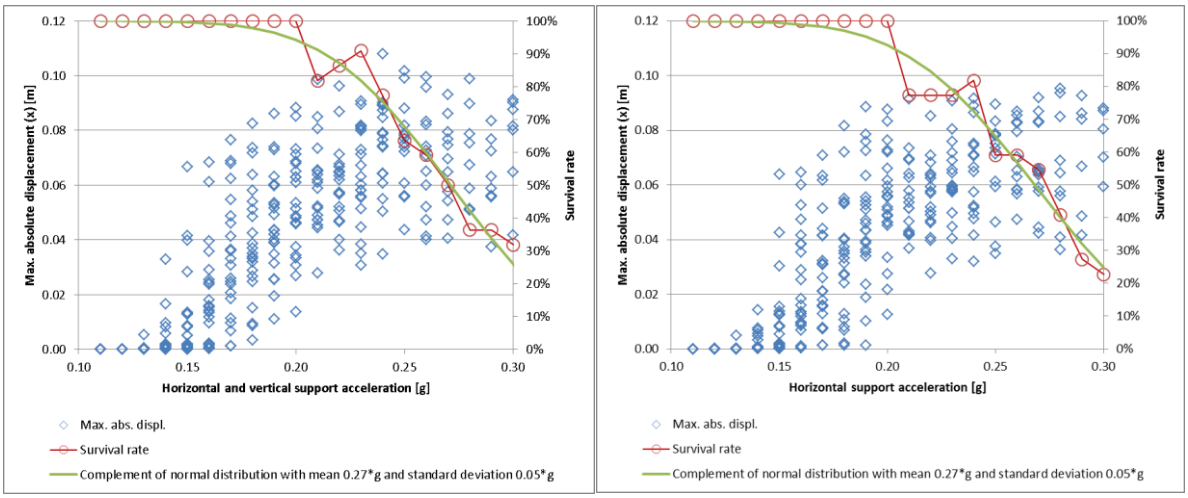

Figure 8. Results from dynamic non-linear kinematic analysis for a straight wall with slenderness 35, thickness 0.1 m, no overburden, coefficient of restitution r_{exp} and subjected to time-histories matching the bedrock spectrum of NPR 9998 (2015). Combinations with simultaneous horizontal and vertical seismic excitation are shown on the left, combinations with only horizontal seismic excitation on the right.

From the obtained fitted cumulative probability functions, it can be inferred that, for this particular case, the Italian NTC (2008) accepts a probability of collapse of 0.2-7% (by taking 0.14g as capacity of the wall) and the New Zealand NZSEE (2016) a probability of collapse of 2-23% (by taking 0.18g as capacity of the wall). These probability ranges are given by the results obtained by using the two different coefficients of restitution, r_{ana} and r_{exp}.

4. DISCUSSION

It is evident that, for the effect of analyzing the global results of the dynamic NLKA in terms of the collapse of the system under the influence of a certain range of scaled ground motions, the choice of coefficient of restitution plays a very significant role (which is why it cannot be said that this model is completely independent of the material properties of the wall). However, it is worth mentioning that in practice the coefficient of restitution will be around the order of r_{exp} or even lower, as it has been

found by several authors. Therefore, it can be said that the probability of collapse is around the order of 0.2% according to NTC (2008) and 2% according to NZSEE (2016).

It is worth mentioning that from a theoretical point of view it is impossible to determine a natural period of vibration of a mechanism due to the absence of stiffness. The effective natural period as determined in static non-linear kinematic analysis is merely an engineering approach to facilitate the quick assessment of the out-of-plane behavior of masonry walls. It is shown that reasonable safety levels are reached in that way, in which the choice of the instability factor is decisive.

Additionally, it was found that out-of-plane displacements greater than the wall thickness (0.10 m in this case) are feasible without collapse, as opposed to the result of an static NLKA. This can be seen in Figure 7 and Figure 8. However, this only happens for a very limited number of applied ground motions, where the acceleration from the earthquake contributes in avoiding the wall collapse.

Finally, although the individual results may vary between the cases where vertical ground motions are applied or not, the global trend of the survival rate as characterized by the normal distribution curves does not seem to be significantly affected by the presence of vertical excitation. It should be noted that in NPR 9998 (2015) the vertical PGA equals the horizontal PGA at bedrock.

5. CONCLUSION

The presented implementation of dynamic non-linear kinematic analysis is a useful tool to assess safety levels that cannot be determined by static non-linear kinematic analysis. By comparing the results of a large number of dynamic kinematic analyses of a masonry wall without overburden having a slenderness of 35 and thickness of 0.10 m to its design capacity as determined by static non-linear kinematic analysis, it turns out that the mean value of its dynamic capacity is greater than the static capacity. The choice of NTC (2008) of factor 0.4 to find the effective natural period of the mechanism is safer in this case than the choice of NZSEE (2016) to use a factor of 0.6, as the first one accepts a smaller probability of collapse than the second one. These probabilities however depend greatly on the choice of coefficient of restitution, which is why certain level of confidence on this factor is suggested (which comes down to certain level of knowledge on the wall material) in order to assess these values with more certainty. By subjecting a masonry wall to the same seismic time-history with increasing PGA, the wall may survive higher PGAs while it can collapse at lower PGAs. This finding may be particularly relevant for laboratory experiments. Furthermore, it should not be taken as a general rule for design purposes as it only occurs under very particular conditions. Vertical seismic loading does not significantly affect the average survival rate of the wall.

6. REFERENCES

Arup (2016). Ground Motions NPR December 2015: Spectrally-matched ground motions for site response and finite element analysis.

Chatzis MN, García Espinosa M, Smyth AW (2017). Examining the energy loss in the inverted pendulum model for rocking bodies. *Journal of Engineering Mechanics*, 143(5).

Consiglio Superiore dei Lavori Pubblici (2008). Istruzioni per l'applicazione delle "Norme Tecniche per le Costruzioni" (NTC) di cui al D.M. 14 gennaio 2008.

Doherty K (2000). An investigation of the weak links in the seismic load path of unreinforced masonry buildings, *Ph.D. Thesis*, Faculty of Engineering, The University of Adelaide, Australia.

Doherty K, Griffith MC, Lam N, Wilson J (2002). Displacement-based seismic analysis for out-of-plane bending of unreinforced masonry walls. *Earthquake Engineering and Structural Dynamics*, 31: 833-850.

Graziotti F, Tomasetti U, Penna A, Magenes G (2016). Out-of-plane shaking table tests on URM single leaf and cavity walls. *Engineering Structures*

Griffith MC, Magenes G, Melis G, Picchi L (2003). Evaluation of out-of-plane stability of unreinforced masonry walls subjected to seismic excitation. *Journal of Earthquake Engineering.*

Housner G (1963). The behavior of inverted pendulum structures during earthquakes. *Bulletin of the Seismological Society of America*, 53(2): 403-417.

Lam NTK, Griffith M, Wilson J, Doherty K (2003). Time-history analysis of URM walls in out-of-plane flexure. *Engineering Structures*, 25: 743-754.

Makris N, Roussos Y (1998). Rocking response and overturning of equipment under horizontal pulse-type motions, Pacific Earthquake Engineering Research Center, PEER-1998/05, University of California, Berkeley.

Nederlands Normalisatie Instituut (2015). Beoordeling van de constructieve veiligheid van een gebouw bij nieuwbouw, verbouw en afkeuren – Grondslagen voor aardbevingsbelastingen: geïnduceerde aardbevingen, Nederlandse praktijkrichtlijn, NPR 9998.

New Zealand Society for Earthquake Engineering NZSEE (2016). The seismic assesment of existing buildings, Technical guidelines for Engineering Assesments, Part C8: Seismic Assessment of Unreinforced Masonry Buildings.

Sorrentino L, Masiani R, Griffith MC (2008). The vertical spanning strip wall as a coupled rocking rigid body assembly," *Structural Engineering and Mechanics.*

Sorrentino L, (2003). Dinamica di muri sollecitati fuori del piano come sistemi di corpi rigidi *Ph.D. Thesis*, Faculty of Engineering, Sapienza University of Rome, Italy.

Yim CS, Chopra A, Penzien J (1980). Rocking Response of Rigid Blocks to Earthquakes. *Earthquake Engineering and Structural Dynamics*, 8: 565-587.